Inorganic Chemistry
Article

Inorg. Chem. **2011**, *50*, 1321–1330 **1321**
DOI: 10.1021/ic101981x

Synthesis, Structure, and Optical Properties of $LiEu(PO_3)_4$ Nanoparticles

R. J. Wiglusz,* R. Pazik, A. Lukowiak, and W. Strek

Institute of Low Temperature and Structure Research, Polish Academy of Sciences, Okolna 2, 50-422 Wroclaw, Poland

Received September 28, 2010

A wet chemical approach was employed for the preparation of $LiEu(PO_3)_4$ nanoparticles. XRD, Raman spectroscopy, TEM, SAED, and IR measurements were used in order to determine the crystal structure and morphology of the obtained product. Complete optical studies including absorption, excitation, emission, and kinetic measurements were performed. At least two components of the $^5D_0 \rightarrow {}^7F_0$ transition were found, indicating the existence of more than one crystallographic position of the Eu^{3+} ions. Asymmetry parameter *R* as well as the covalence of the Eu−O bond were found to decrease with the grain growth.

Introduction

Advanced synthesis techniques for new luminescent materials with designed optical properties provide great potential in the field of modern optoelectronic applications.[1−3] Among a variety of mixed oxide materials doped with d or f metal cations, the tetraphosphate family is widely studied due to its outstanding optical properties, finding applications in the constantly growing market of phosphors, optical fibers, and scintillators.[4−6] These polyphosphates are described by the general formula $M^IM^{III}(PO_3)_4$, where M^I is alkali metal and M^{III} represents lanthanide ions such as Eu^{3+}, Nd^{3+}, Gd^{3+}, Pr^{3+}, etc. The structural unit of polyphosphate is based on a PO_4 group usually constituted of $(-PO_3-O-PO_3-O-)_n$ chains.[7] Different modes of condensation lead to the formation of several interesting structural compounds.[8−11] It must be underlined that the optical properties of these compounds are strongly dependent on the nature of the lanthanide dopants and the structure of the host matrix.[12] For instance, Yamada emphasized that a relatively large distance between neighboring Nd ions in $LiNd(PO_3)_4$ (5.6636(12) Å) prevents nonradiative concentration quenching.[13] The same observation regarding an extremely long distance between lanthanides in the $LiLn(PO_3)_4$ single crystals (Ln−Eu^{3+}, La^{3+} and Gd^{3+}) was found by Zhu et al.[14] Hong[15] and Koizumi[16] studied the crystal structures of $LiNd(PO_3)_4$ and $NaNd(PO_3)_4$ and showed that these systems are suitable for low threshold laser materials. Parreu et al.[17] investigated $KLn(PO_3)_4$ crystals, mainly with Nd^{3+} and Gd^{3+}, and explored their ability to generate the second harmonic of a laser beam. Moreover, $LiLa(PO_3)_4$ polyphosphates doped mutually with Yb^{3+} and Er^{3+} could find application as eye-safe lasers.[18]

In this article, we focus on the synthesis and structural and optical characterization of the $LiEu(PO_3)_4$ nanoparticles obtained by wet chemistry synthesis.[19] Among all of the lanthanides, Eu^{3+} is most commonly used in luminescence studies due to its narrow band emission and the long lifetimes of the excited states. Moreover, Eu^{3+} doping allowed for the extraction of necessary information regarding the local environment of lanthanide and the structure directly from the emission spectra. Detailed characterization of the luminescence properties of the $LiEu(PO_3)_4$ nanoparticles was performed on the basis of absorption, excitation, and emission spectra. Splitting of the Eu^{3+} $^5D_0 \rightarrow {}^7F_0$ electron transition was used in order to determine the symmetry of the occupied position of the dopant within the crystal structure of the host

*To whom correspondence should be addressed. Phone: +48-71-343-50-21. Fax: +48-71-344-10-29. E-mail: R.Wiglusz@int.pan.wroc.pl.

(1) Campayo, L.; Audubert, F.; Bermache-Assollant, D. *Solid State Ionics* **2005**, *176*, 2663.
(2) Malinowski, M.; Strek, W. *J. Phys. C* **1987**, *20*, 2595.
(3) Szczygiel, I. *Solid State Sci.* **2005**, *7*, 189.
(4) Cole, J. M.; Lees, M. R.; Howard, J. A. K.; Newport, R. J.; Saunders, G. A.; Schönherr, E. *J. Solid State Chem.* **2000**, *150*, 377.
(5) Ferid, M.; Horchani-Naifer, K. *Solid State Ionics* **2005**, *176*, 1949.
(6) Farok, H. M.; Senin, H. B.; Saunders, G. A.; Poon, W.; Vass, H. *J. Mater. Sci.* **1994**, *29*, 2847.
(7) Barsukov, I. V.; Syt'ko, V. V.; Umreiko, D. S. *J. Appl. Spectrosc.* **2004**, *71*, 676.
(8) Hamady, A.; Jouini, T. *Acta Crystallogr., Sect. C* **1996**, *52*, 2949.
(9) Hong, H.Y.-P.; Chinn, S. R. *Mater. Res. Bull.* **1976**, *11*, 421.
(10) Rekik, W.; Naïli, H.; Mhiri, T. *Acta Crystallogr., Sect. C* **2004**, *60*, i50.
(11) Szczygiel, I. *Thermochim. Acta* **2004**, *417*, 75.
(12) Akrim, A.; Zambon, D.; Metin, J.; Cousseins, J. C. *Eur. J. Solid State Inorg. Chem.* **1993**, *30*, 483.
(13) Yamada, T.; Otsuka, K.; Nakano, J. *J. Appl. Phys.* **1974**, *45*, 5096.
(14) Zhu, J.; Cheng, W.-D.; Wu, D.-S.; Zhang, H.; Gong, Y.-J.; Tong, H.-N.; Zhao, D. *Eur. J. Inorg. Chem.* **2007**, *2*, 285.
(15) Hong, H.Y.-P. *Mater. Res. Bull.* **1975**, *10*, 635.
(16) Koizumi, H. *Acta Crystallogr., Sect. B* **1976**, *32*, 2254.
(17) Parreu, I.; Carvajal, J. J.; Solans, X.; Diaz, F.; Aguilo, M. *Chem. Mater.* **2006**, *18*, 221.
(18) Obaton, A. F.; Parent, C.; Le Flem, G.; Thony, P.; Brenier, A.; Boulon, G. *J. Alloys Compd.* **2000**, *300−301*, 123.
(19) Wiglusz, R. J.; Bednarkiewicz, A.; Lukowiak, A.; Strek, W. *Spectrosc. Lett.* **2010**, *43*, 1.

Published on Web 01/18/2011

matrix. The Judd−Ofelt theory was applied to calculate the radiative properties of the prepared materials. Moreover, the asymmetry ratio between the $^5D_0 \rightarrow {}^7F_2$ and $^5D_0 \rightarrow {}^7F_1$ electron transitions was calculated.

Experimental Section

The preparation of $LiEu(PO_3)_4$ nanoparticles was based on the general principles of wet chemistry used by us previously for the synthesis of hydroxyapatites.[19] As starting materials, $(NH_4)_2HPO_4$ (POCH), Eu_2O_3 (Sigma Aldrich), and Li_2CO_3 (POCH) with purities of 99.99% were chosen. Calculated and stoichiometric amounts of Eu_2O_3 (5 mmol) and Li_2CO_3 (5 mmol) were digested in an excess of diluted HNO_3 in order to transform them into nitrate salts. $(NH_4)_2HPO_4$ (40 mmol) was dissolved in MQ-water and subsequently mixed with the obtained nitrates containing appropriate amounts of Eu^{3+} and Li^+, resulting in a homogeneous solution. The ongoing synthesis could be divided into two major steps: the first, precipitation of the amorphous polyphosphate and, the second, transformation of the amorphous product into a crystalline one via thermal treatment. The former reaction could be written as follows:

$$LiNO_3 + Eu(NO_3)_3 + 4(NH_4)_2HPO_4 \xrightarrow{pH8-9} LiEu(PO_3)_{4(amorph)} + 4NH_4NO_3 + 4NH_4OH \quad (1)$$

and the latter one as

$$LiEu(PO_3)_{4(amorph)} \xrightarrow{600-800°C/8h} LiEu(PO_3)_{4(cryst)} \quad (2)$$

Afterward, the raw mixture was subjected to thermal treatment using an electric furnace at a temperature of 600−800 °C for 8 h. As a result of the annealing process, white powders of $LiEu(PO_3)_4$ were obtained and kept in glass vials sealed with parafilm in order to protect them from possible contamination and the adsorption of impurities on the surface of the nanoparticles.

Apparatus. The XRD patterns were collected at room temperature on a Stoe STADI P transmission diffractometer in Debye−Scherrer geometry equipped with a linear position sensitive detector using Cu Kα1 radiation (1.54060 Å). The $LiEu(PO_3)_4$ powders were investigated with transmission electron microscopy (TEM) using a Philips CM-20 SuperTwin microscope, operating at 200 kV. Specimens for HRTEM were prepared by dispersing a small amount of the sample in methanol and putting a droplet of the suspension on a copper microscope grid covered with perforated carbon. Raman spectroscopy was done using a LabRam HR 800 Horiba Yvon Jobin equipped with a 9 mW HeNe laser emitting a 632.8 nm line. The optical absorption spectra were obtained using a Cary-Varian 5E UV−Vis−near-IR spectrophotometer in the 180−2400 nm spectral region. The IR measurements were performed using an FT-IR Biorad 575C spectrophotometer. The luminescence spectra were recorded using a Jobin Yvon THR1000 monochromator equipped with a Hamamatsu R928 photomultiplier and a 1200 L/mm grating blazed at 500 nm. As an excitation source, the continuous 266 nm line of a YAG:Nd laser (third harmonics) was used. Excitation spectra were measured using a 450 W xenon arc lamp coupled with a 275 mm excitation Spectra Pro 750 monochromator which used a 1800 L/mm grating blazed at 250 nm. The lifetimes were measured utilizing a LeCroy oscilloscope after 266 nm excitation with a pulse YAG:Nd laser (266 nm). The decay curve deconvolution was done with the PSIPLOT software. All recorded spectra were corrected according to the apparatus characteristics.

Results and Discussion

Structural Analysis. The formation of crystalline $LiEu(PO_3)_4$ nanopowders was followed by XRD measurements (see Figure 1). All of the samples prepared utilizing wet chemistry techniques showed detectable crystallinity at all ranges of proposed sintering temperatures (600−800 °C). A comparison of the resulting diffraction patterns with the reference standard of $LiEu(PO_3)_4$ (JCPDS 34−1360) confirms the presence of a single phase, monoclinic structure (C12/c1(15)) in the final product.[20] The structure of $LiEu(PO_3)_4$ is commonly described as a 3-D framework built up of $(PO_4)^{3-}$ zigzag chains and infinite chains constituted of EuO_8 as well as LiO_4 polyhedra. The Eu^{3+} is surrounded by eight oxygen atoms forming dodecahedra, with the symmetry site of the Eu^{3+} position being depicted as C_{2v}.[7] The projection of the structure along the b axis is shown in Figure 2 accordingly to Zhu et al.[14] The mean size of the crystallites was estimated from the broadening of the diffraction peaks using Scherrer's well-known equation:

$$D = \frac{k\lambda}{\cos\Theta\sqrt{\beta^2 - \beta_0^2}} \quad (3)$$

where D is the grain size, β_0 is the apparatus broadening, β is the full width at half maximum, Θ is the diffraction angle, k is the constant (usually equal to 0.9), and λ is the X-ray wavelength.[21] Depending on the annealing temperature, the average grain size varies slightly from 33 nm (at 600 °C) to 43 nm (at 800 °C). In the case where the sample was heat-treated at 700 °C, the grain size was in the intermediate range around 36 nm. The cell parameters were calculated with the help of Rietveld analysis[22] using an isotropic approach[23] and the Maud 2.0 software.[24] Results of the calculations are gathered in Table 1. The observed general trend is as follows: all unit cell parameters decrease with an increase in the annealing temperature or, in other words, with an increase in the grain size. The significant difference between the unit cell parameters of the $LiEu(PO_3)_4$ single crystal and those of the nanoparticles, higher values for all of them in the latter case, is caused by the so-called grain size effect. Reduction of the particle size contributes to the creation of negative pressure on the crystal lattice and leads directly to a lattice cell volume expansion.[25,26] Actually, this behavior was one of the features expected as a result of reducing the grain size.

According to the TEM study (Figure 3a), the particles of $LiEu(PO_3)_4$ sintered at 800 °C are elongated, reminiscent of the shape of flat plates and forming large groups of agglomerates with an average size of 200 nm. However, it is possible to define the primary size of the particles being around 30−50 nm, which goes well with the calculation using Scherrer's equation. Analysis of the SAED image (Figure 3b) reveals the presence of very sharp, individual

(20) Chudinova, N. N.; Vinogradova, V. N. *Inorg. Mater.* **1979**, *15*, 1706.
(21) Klug, P.; Alexander, L. E. *X-ray Diffraction Procedure*; Wiley: New York, 1954.
(22) Rietveld, H. M. *J. Appl. Crystallogr.* **1969**, *2*, 65.
(23) Delhez, R.; de Keijser, T. H.; Langford, J. I.; Louër, D.; Mittemeijer, E. J.; Sonneveld, E. J. Crystal Imperfection Broadening and Peak Shape in the Rietveld Method. In *The Rietveld Method*; Young, R.A., Eds.; Oxford Science: Oxford, United Kingdom, 1993; p 132.
(24) Lutterotti, L.; Matthies, S.; Wenk, H.-R. *IUCr: Newslett. CPD* **1999**, *21*, 14.
(25) Palkar, V. R.; Ayyub, P.; Chattopadhyay, S.; Multani, M. *Phys. Rev. B* **1996**, *53*, 2167.
(26) Ayyub, P.; Palkar, V. R.; Chattopadhyay, S.; Multani, M. *Phys. Rev. B* **1995**, *51*, 6135.

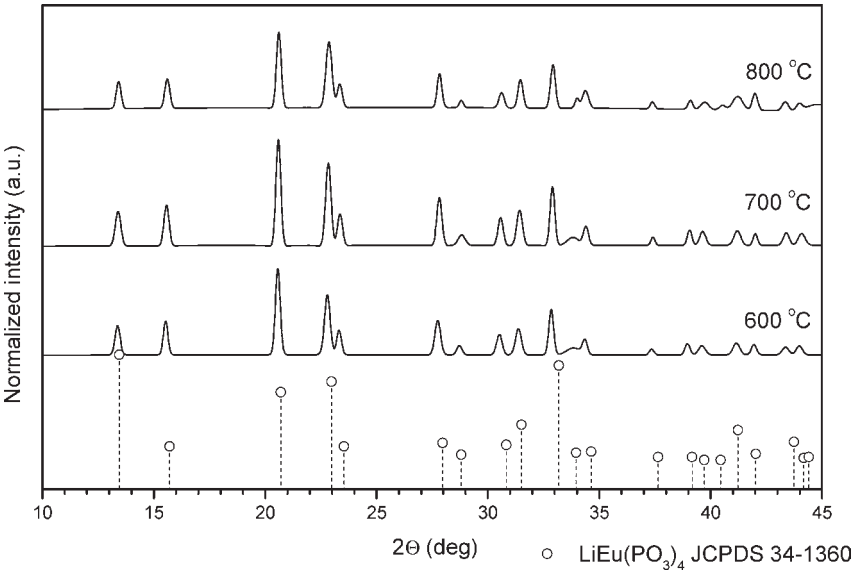

Figure 1. XRD patterns of $LiEu(PO_3)_4$ nanoparticles as function of thermal treatment.

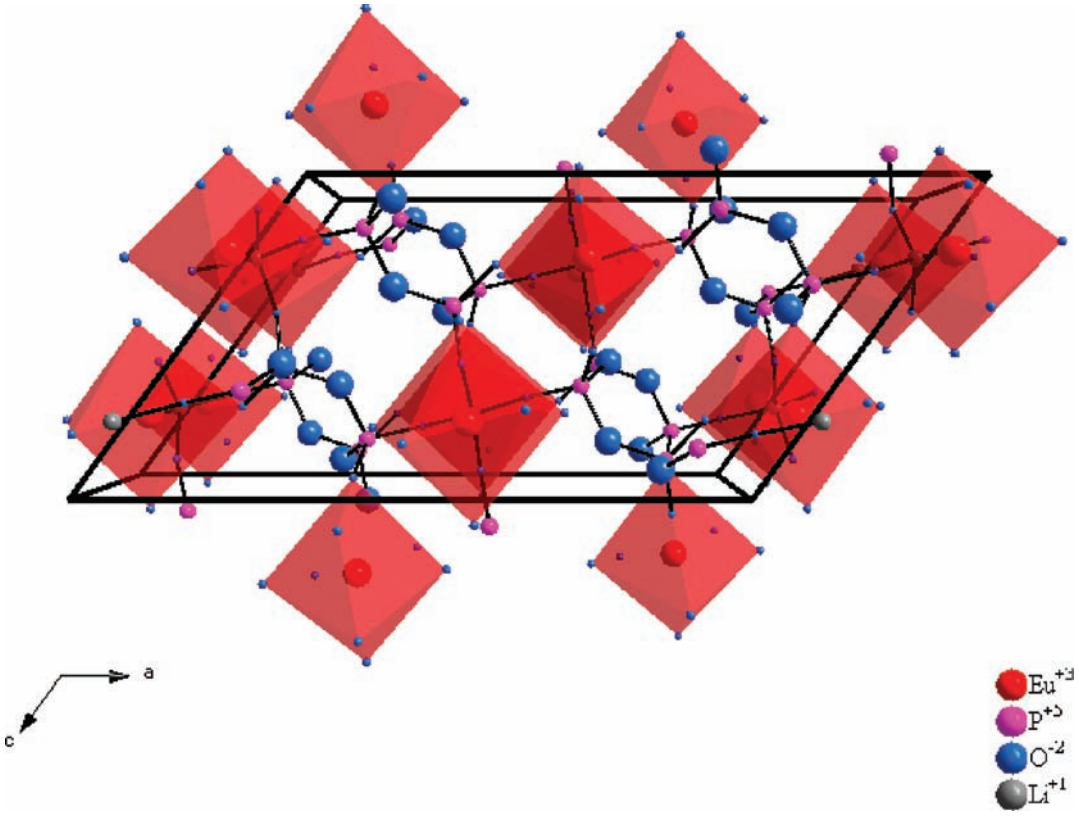

Figure 2. Projection of the $LiEu(PO_3)_4$ structure along the *b* axis.

Table 1. Unit Cell Parameters of the $LiEu(PO_3)_4$ Nanoparticles

T (°C)	*a* (Å)	*b* (Å)	*c* (Å)	*β* (deg)	volume (Å^3)
single crystal[a]	16.300(9)	7.0330(4)	9.6465(6)	126.14(3)	894.7(0)
600	16.3559(7)	7.0471(3)	9.6635(4)	126.11497(5)	899.82(131)
700	16.3533(7)	7.0447(3)	9.6626(4)	126.118(2)	899.22(131)
800	16.353(1)	7.0451(4)	9.6627(7)	126.129(3)	899.14(197)

[a] Data for the single crystal taken from ref 14.

spots from crystalline particles at positions corresponding to the monoclinic phase of $LiEu(PO_3)_4$.

The results of Raman spectroscopy (see Figure 4) revealed the presence of typical modes at 701 cm^{-1} and

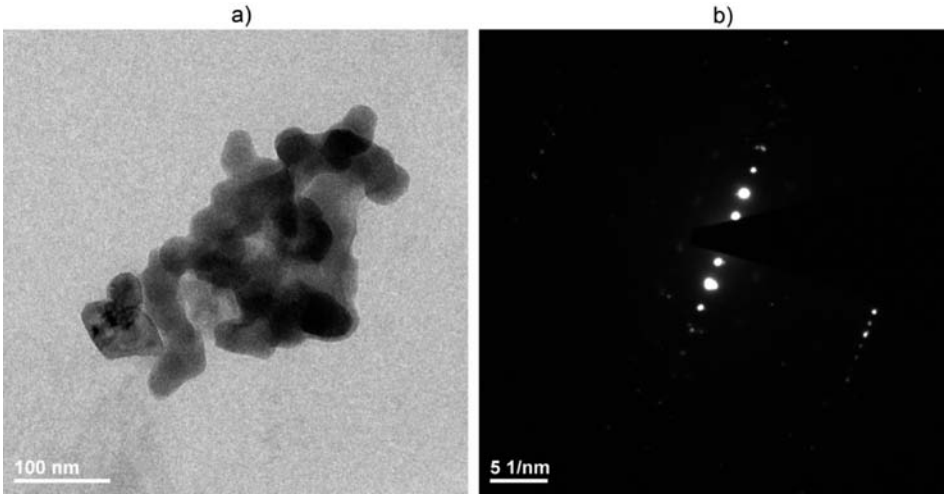

Figure 3. TEM (a) and SAED diffraction (b) images of the $LiEu(PO_3)_4$ nanoparticles prepared at 800 °C.

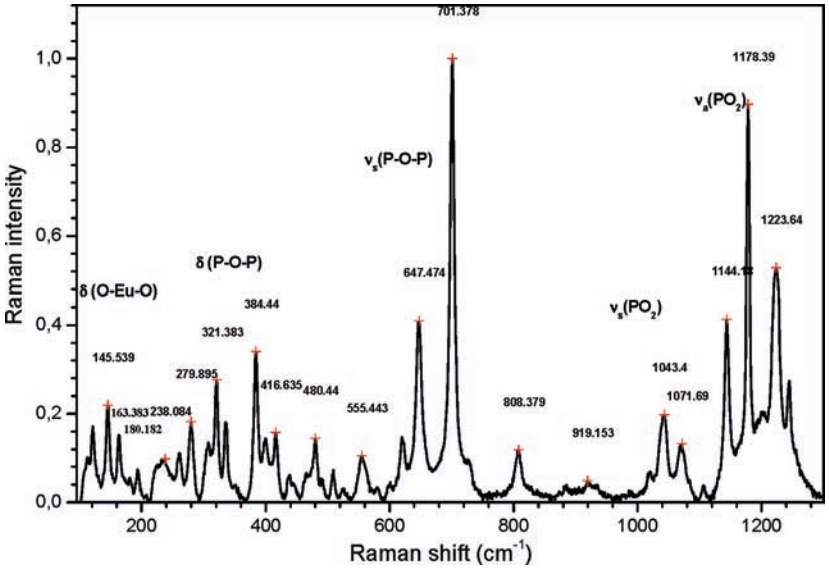

Figure 4. Room temperature Raman spectra of the $LiEu(PO_3)_4$ heated at 800 °C.

1178 cm^{-1} and other signals of $LiEu(PO_3)_4$, confirming the structure of the prepared materials.[27] All bands, with a similar appearance in the spectra (frequencies and shapes), were observed as well for the iso-structural chain type structures of polyphosphates such as $LiCe(PO_3)_4$ and $KCe(PO_3)_4$,[27] whereas signals of polyphosphates crystallizing in cyclic forms should appear at around 800 cm^{-1} and 1220 cm^{-1} like, for instance, in $KDy(PO_3)_4$.[27] The complete modes assignment is gathered in Table 2.

Optical Properties. The reflectance absorption spectra were measured at room temperature, covering the spectral region of 200−700 nm, and were corrected according to the Kubelka−Munk equation.[28] Figure 5 presents the representative results of the measurements for the $LiEu(PO_3)_4$ nanocrystalline sample sintered at 800 °C. In the region of 200−300 nm, the spectra consist of high intensity bands corresponding to the charge transfer (C-T) transitions between Eu^{3+} and O^2 and overlapping 4f → 5d transitions of Eu^{3+}.[29] Above 350 nm, one may observe absorption ascribed to the f−f optical transitions from the $^7F_0$ and $^7F_1$ levels to the excited states of Eu^{3+}. The appearance of the absorption bands from $^7F_1$ is due to the significant thermal population of this level at room temperature.[30]

The excitation spectra of $LiEu(PO_3)_4$ (see Figures 6 and 7) were measured at room and liquid nitrogen temperatures at a recorded emission wavelength of 615 nm corresponding to the $^5D_0 \rightarrow {}^7F_2$ electron transition. The abundance of sharp and intense absorption lines ascribed to the transitions from $^7F_0$ to $\{^5H_{6,5,4,7,3}\}$ (318 nm), $\{^5G_{6,5,4}\}$ (363 nm), $\{^5G_2, {}^5L_7, {}^5G_3\}$ (381 nm), $^5L_6$ (394 nm), $^5D_2$ (465 nm), $^5D_1$ (525 nm), and $^5D_0$ (590 nm), as well as from $^7F_1$ and $^7F_2$ to $^5D_1$ (535 and 552 nm), could be clearly seen in the spectra. However, the rather complex

(27) Dammak, T.; Fourati, N.; Abid, Y.; Mlayah, A.; Minot, C. *THEOCHEM* **2008**, *852*, 83.
(28) Zhang, Q.; Zhang, Z.; Zhou, Z. *Appl. Phys. B: Laser Opt.* **2008**, *93*, 589.
(29) Matraszek, A.; Macalik, L.; Szczygieł, I.; Godlewska, P.; Solarz, P.; Hanuza, J. *J. Alloys Compd.* **2008**, *451*, 254.
(30) Babu, S. S.; Babu, P.; Jayasankar, C. K.; Sievers, W.; Tröster, Th.; Wortmann, G. *J. Lumin.* **2007**, *126*, 109.

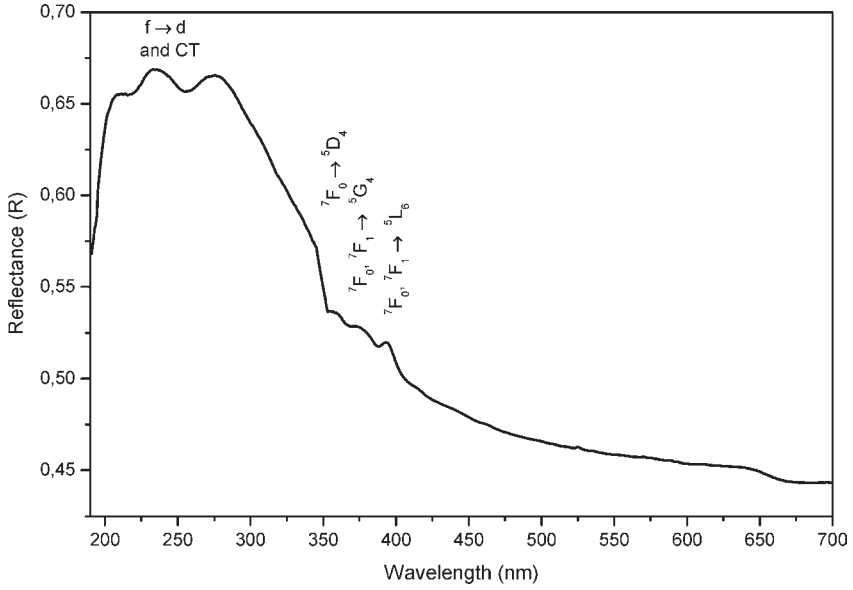

Figure 5. Reflectance absorption spectra of $LiEu(PO_3)_4$ heated at 800 °C and recorded at 300 K.

Table 2. Vibronic Components on the Emission Spectra of $LiEu(PO_3)_4$ ($^5D_0 \rightarrow {}^7F_0$ and $^5D_0 \rightarrow {}^7F_2$)

		ΔE (from 0-phonon line)		
transitions	energy [cm^{-1}]	**1**	**2**	**3**
$^5D_0 \rightarrow {}^7F_0$	17296(1)			
	17151	$145_{\delta(O-Eu-O)}$		
	17116	$180_{\delta(O-Eu-O)}$		
	17081	$215_{\delta(O-Eu-O)}$		
$^5D_0 \rightarrow {}^7F_2$	16379(2)			
	16363	$933_{\nu s(PO2)}$		
	16341(3)			
	16253	$1043_{\nu s(PO2)}$	$126_{\delta(O-Eu-O)}$	
	16225	$1071_{\nu s(PO2)}$	154	
	16193		186	
	16174			
	16152	$1144_{\nu a(PO2)}$		
	16118	$1178_{\nu a(PO2)}$	$261_{\delta(P-O-P)}$	
	16073	$1223_{\nu a(PO2)}$	$306_{\delta(P-O-P)}$	$268_{\delta(P-O-P)}$

shape of the spectra has been caused by thermal population of the $^7F_{1,2}$ levels as well as electron−phonon coupling. One of the interesting features found in the excitation spectra, especially for the sample treated at 800 °C, is the appearance of two lines ascribed to the $^7F_0 \rightarrow {}^5D_0$ absorption transition, indicating more than one crystallographic position for the Eu^{3+} ions to locate. The variance of the line shapes and peak numbers might be caused by the lower level of sample crystallization and different cell parameters affecting the crystal field; splitting of Eu^{3+} levels, local distortions of the closest surrounding of Eu^{3+}, as well as the overlap of the excitation bands of Eu^{3+} ions localized in different sites may be hypothesized as well.

The 266 nm excited emission spectra of the $LiEu(PO_3)_4$ nanoparticles were recorded at 300 and 77 K (Figures 8 and 9) as a function of the thermal treatment. All of the resulting spectra were normalized. The emission spectra consist of the characteristic bands in the visible region ascribed to the specific electron transitions occurring within the f−f shell of Eu^{3+}. The $^5D_0 \rightarrow {}^7F_{0-4}$ transitions resulting from the emission from the first excited $^5D_0$ level to the crystal field components of the $^7F_{0-4}$ levels of the ^7F ground term were clearly seen. Further lying transitions like $^5D_0 \rightarrow {}^7F_{5,6}$ usually are rarely detected due to their low intensity. The $^5D_0 \rightarrow {}^7F_0$ transition is located at 579 nm, $^5D_0 \rightarrow {}^7F_1$ at 590 nm, $^5D_0 \rightarrow {}^7F_2$ at 615 nm, $^5D_0 \rightarrow {}^7F_3$ at 650 nm, and $^5D_0 \rightarrow {}^7F_4$ at 700 nm. The spectra are quite similar to the behavior of that of the single crystal of $LiEu(PO_3)_4$ reported by Zhu et al.,[14] but few differences could be noticed. First of all, since the ground state $^7F_0$ and the first excited level of $^5D_0$ of Eu^{3+} are non-degenerated under any symmetry, analysis of this line could provide information about the existence of the number of crystallographic sites occupied by optically active ions in the crystalline network. In the presented emission spectra (see inset in Figure 8), one could distinguish at least three components of $^5D_0 \rightarrow {}^7F_0$, suggesting that Eu^{3+} occupied more than one position in the structure, instead of only one position as found in the $LiEu(PO_3)_4$ single crystal. This conclusion was supported by the appearance of at least two peaks corresponding to the $^7F_0 \rightarrow {}^5D_0$ absorption transition in the excitation spectra (see Figure 6). Moreover, the line position is slightly blue-shifted at 17 270 cm^{-1} (579 nm) in contrast to the single crystal, where it can be found at 17 182 cm^{-1} (582 nm). These two features, especially the latter one, could be connected with a well-known "size effect" that manifests itself in the change of crystal field that further affects both the energy level splitting and the band gap. That, in turn, is of great importance in the engineering of new optical materials like quantum dots (QDs).[31] Nevertheless, due to the shielding of the f electrons in lanthanides, the observed changes are not expected to be as significant as in the QDs. The former phenomena could be explained by the presence of defects in the crystal structure of nanoparticles and as a result of the number of Eu^{3+} ions occupying unexpected crystallographic sites, characterizing different local symmetry.

(31) Li, J. W.; Yang, L. W.; Zhou, Z. F.; Chu, P. K.; Wang, X. H.; Zhou, J.; Li, L. T.; Sun, C. Q. *J. Phys. Chem. C* **2010**, *114*, 13370.

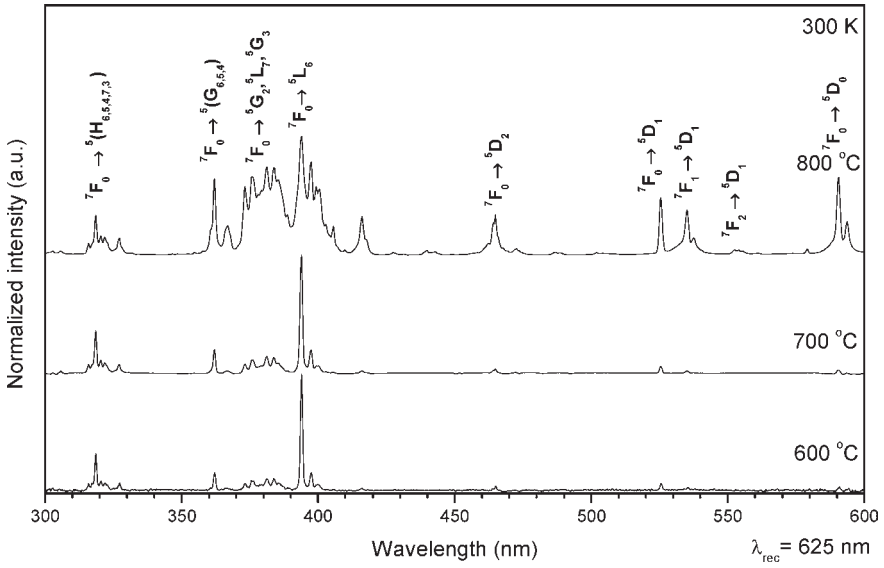

Figure 6. Excitation spectra of $LiEu(PO_3)_4$ measured at 300 K as a function of the annealing temperature.

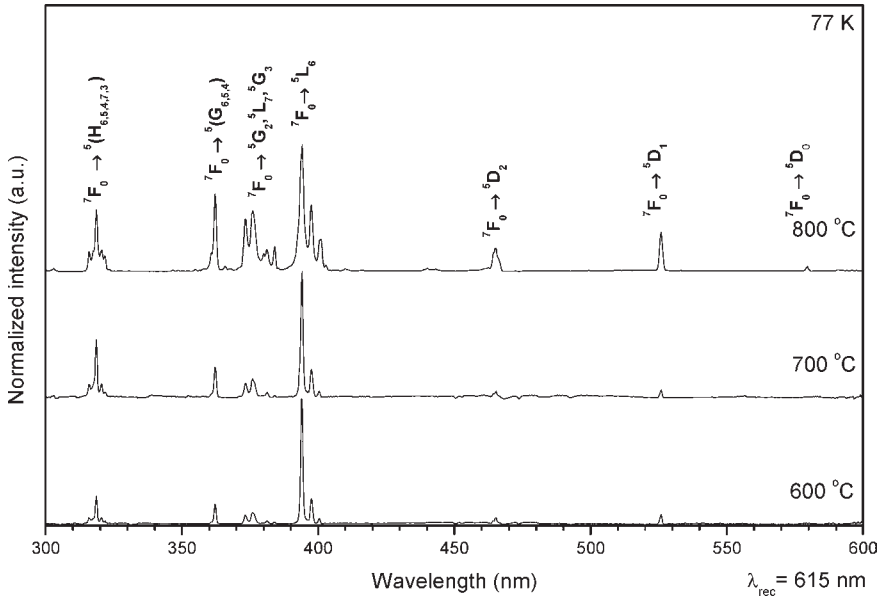

Figure 7. Excitation spectra of $LiEu(PO_3)_4$ heated at 800 °C measured at 77 K as a function of the annealing temperature.

In the case of all examined samples, the ^7F_J multiplet of Eu^{3+} is split into the maximum number of Stark sublevels, pointing out not only overlapping of the peaks, related to the differently placed Eu^{3+} ions in the structure, but also, to a large extent, the low symmetry C_{2v} of the optically active center. The Rietveld analysis supported this fact, suggesting that the Eu^{3+} coordination is close to a distorted tricapped trigonal prism (TCTP). Moreover, the occurrence of the nondegenerated $^5D_0 \rightarrow {}^7F_0$ transition is directly related with the existence of low symmetry surroundings of Eu^{3+} in the studied samples.[32]

The intensities of the magnetic dipole allowed $^5D_0 \rightarrow {}^7F_1$. The electric dipole allowed $^5D_0 \rightarrow {}^7F_2$, and $^5D_0 \rightarrow {}^7F_4$ transitions are comparable, which generally indicates a lack of $J-J$ mixing.[18] It is important to emphasize that the magnetic dipole transition was practically independent of the host matrix and thus could be treated as a kind of internal reference. On the other hand, the electric dipole transition remains extremely sensitive to even slight changes of the local environment of Eu^{3+}. Generally, when the Eu^{3+} ions occupy crystallographically different positions, the magnetic dipole transition $^5D_0 \rightarrow {}^7F_1$ is allowed, whereas in the noncentrosymetric site, the electric dipole transition $^5D_0 \rightarrow {}^7F_2$ becomes predominant.[33] It is well-known that the asymmetry ratio

$$R = \frac{I(^5D_0 \rightarrow {}^7F_2)}{I(^5D_0 \rightarrow {}^7F_1)} \quad (4)$$

(32) Brito, H. F.; Malta, O. L.; Alves de Carvalho, C. A.; Menezes, J. F. S.; Souza, L. R.; Fenaz, R. *J. Alloys Compd.* **1998**, *275*−*277*, 254.

(33) Bünzli, J. C. G.; Choppin, G. R. *Lanthanide Probes in Life Chemical and Earth Sciences. Theory and Practice*; Elsevier: Amsterdam, 1979; Chapter 35.

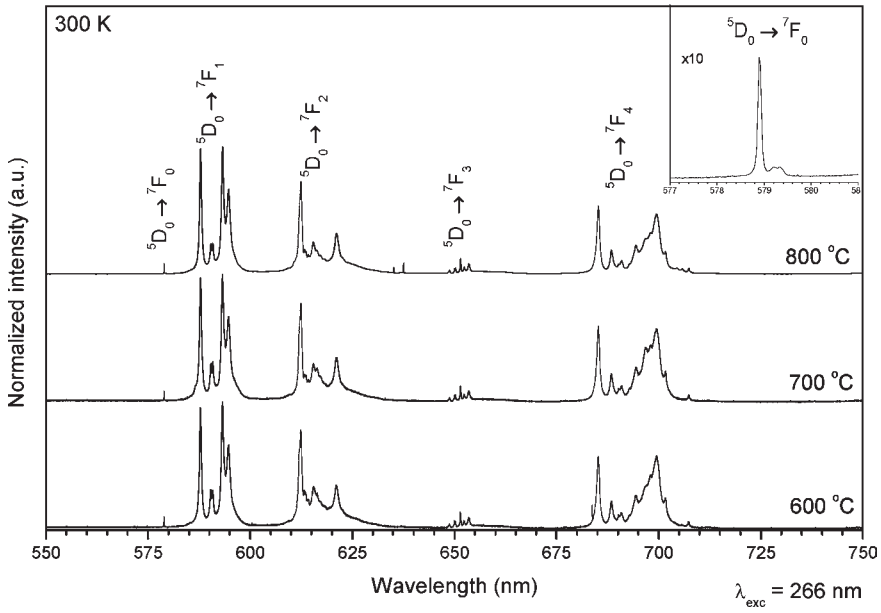

Figure 8. Emission spectra of $LiEu(PO_3)_4$ as a function of the sintering temperature measured at 300 K.

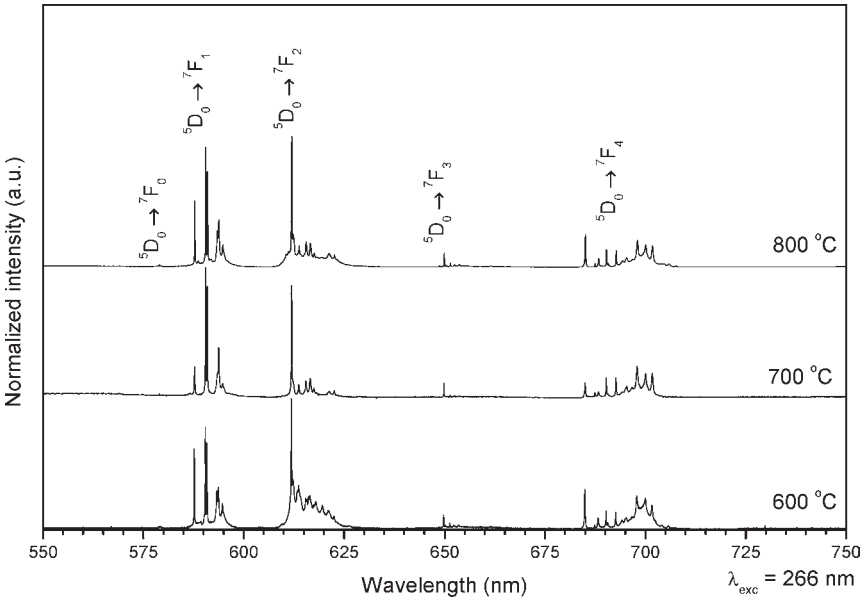

Figure 9. Emission spectra of $LiEu(PO_3)_4$ as a function of the sintering temperature measured at 77 K.

of integrated intensities of the $^5D_0 \rightarrow {}^7F_2$ and $^5D_0 \rightarrow {}^7F_1$ transitions can be considered indicative of the asymmetry of the coordination polyhedron of the Eu^{3+} ion. Thus, in this sense, the higher the I_{0-2}/I_{0-1} ratio is, the more apart from a centrosymmetric geometry Eu^{3+} is located.[34] In fact, the asymmetry parameter R of $LiEu(PO_3)_4$ decreases with an increase in the sintering temperature from 1.08 ± 0.054 to 0.88 ± 0.04 (see Table 3). Hence, the local environment of Eu^{3+} showed a relatively small degree of distortion at 300 K.

The superposition of the Raman and emission spectra allowed for possible elucidation of the vibronic components and proves strong electron−phonon coupling in the range of appearance of the $^5D_0 \rightarrow {}^7F_2$ transition (see Table 2). However, it is possible that in the range of the $^5D_0 \rightarrow {}^7F_{1,2}$ transitions, resonance could occur as well. The intensities of the vibronic transitions could be in principle evaluated from the temperature dependence of the absorption bands. According to the theory of vibronic transition probabilities, electron−phonon coupling is mainly operative for transitions obeying the $\Delta J = 2$ selection rule.

For a more detailed investigation of the nature of the luminescence behavior of Eu^{3+} in $LiEu(PO_3)_4$, the intensity parameters Ω_2 and Ω_4 were determined using the approaches described previously by Kodaira et al.,[35] Werts et al.,[36] and

(34) Oomen, E. W. J. L.; van Dongen, A. M. A. *J. Non-Cryst. Solids* **1989**, *111*, 205.

(35) Kodaira, C. A.; Brito, H. F.; Malta, O. L.; Serra, O. A. *J. Lumin.* **2003**, *101*, 11.

(36) Werts, M. H. V.; Jukers, R. T. F.; Verhoeven, J. W. *Phys. Chem. Chem. Phys.* **2002**, *4*, 1542.

Table 3. Decay Rates of Radiative (A_{rad}), Nonradiative (A_{nrad}), and Total (A_{tot}) Processes of $^5D_0 \rightarrow {}^7F_J$ Transitions; Luminescence Lifetimes (τ); Intensity Parameters (Ω_2, Ω_4); and Asymmetry Ratio (R) Determined from Photoluminescence Spectra of the $LiEu(PO_3)_4$ Nanopowders as a Function of the Sintering Temperature

sample	A_{rad} [s^{-1}]	A_{nrad} [s^{-1}]	A_{tot} [s^{-1}]	τ [ms]	Ω_2 [10^{-20} cm^2]	Ω_4 [10^{-20} cm^2]	η [%]	R
600 °C	187.98	516.25	704.23	1.42	1.21	3.67	26.69	1.07
700 °C	178.49	427.57	606.06	1.65	1.04	3.60	29.45	1.08
800 °C	163.93	376.61	540.54	1.85	0.96	3.11	30.32	0.88

Hreniak et al.[37] Correct Judd−Ofelt (JO) calculations can be done only for RE ions in a well-defined crystallographic structure where energy transfer between ions in different sites does not occur. In order to determine the Ω_λ parameters, we have used the relation between the $^5D_0 \rightarrow {}^7F_J$ transitions assuming that the matrix element $U^{(6)}$ is close to zero for the $^5D_0 \rightarrow {}^7F_6$ transition ($U^{(6)} = 0.0005$). Thus, matrix elements for transitions starting from ^5D_J ($J = 0$, 1, 2, and 3) are zero.[38] The Einstein coefficient $A_{0-\lambda}$ for spontaneous emission can be expressed as

$$A_{0-\lambda} = \frac{64\pi^4\nu^3e^2}{3hc^3}\frac{1}{4\pi\varepsilon_0}\chi\sum_{\lambda=2,4}\Omega_\lambda\langle {}^5D_0\|U^{(\lambda)}\|F_J\rangle^2 \quad (5)$$

Moreover, due to "clearing" matrix elements $U^{(4)}$ and $U^{(6)}$ and elements $U^{(2)}$ and $U^{(6)}$ for the $^5D_0 \rightarrow {}^7F_2$ and $^5D_0 \rightarrow {}^7F_4$ transitions, respectively, we can get the values of Ω_2 and Ω_4 by determining $A_{0-\lambda}$ directly from emission spectra, taking $\langle {}^5D_0\|U^{(2)}\|{}^7F_2\rangle = 0.0035$ and $\langle {}^5D_0\|U^{(4)}\|{}^7F_4\rangle = 0.0030$. It can be done by using the relation between the integral intensity I and the transition energy $h\nu$ given as $I = h\nu AN$, where A is the Einstein coefficient for spontaneous emission and N is the population of the emitting $^5D_0$ level. Comparing both sides of the equations for the $^5D_0 \rightarrow {}^7F_2$ and $^5D_0 \rightarrow {}^7F_4$ transitions to N, the expression for $A_{0-\lambda}$ can be rewritten as

$$A_{0-\lambda} = A_{0-J} = A_{0-1}\frac{I_{0-J}}{I_{0-1}}\frac{h\nu_{0-1}}{h\nu_{0-J}} \quad (6)$$

where I_{0-J} and $h\nu_{0-J}$ and I_{0-1} and $h\nu_{0-1}$ are the integral intensities and energies for $^5D_0 \rightarrow {}^7F_J$ and $^5D_0 \rightarrow {}^7F_1$ transitions, respectively. The value of the A_{0-1} coefficient corresponding to the $^5D_0 \rightarrow {}^7F_1$ transition was taken to be equal to 50 s^{-1} due to the magnetic character of the $^5D_0 \rightarrow {}^7F_1$ transition and its weak dependence on the crystal field effects. Following the magnitudes of decay rates ($A_{J-J'}$) determined from the excited $^5D_0$ level, it is possible to evaluate the radiative decay rate (A_{rad}):

$$A_{rad} = \sum_{J'} A_{J-J'} \quad (7)$$

Additionally, by taking measured luminescence lifetimes, one can calculate the nonradiative (A_{nrad}) and total decay rates (A_{tot}) from the following equation:

$$A_{tot} = \frac{1}{\tau} = A_{rad} + A_{nrad} \quad (8)$$

Finally, one can also determine the quantum efficiency of overall luminescence as

$$\eta = \frac{A_{rad}}{A_{rad} + A_{nrad}} \quad (9)$$

One can note that the magnitudes of both Ω_2 and Ω_4 parameters decrease with an increase in the annealing temperature almost in the same way, but this behavior is more pronounced for Ω_2 parameters. One could conclude that transitions induced by a change of the electric dipole decrease with an increase of the sintering temperature or with an increase of the grain size and crystallinity level of the final product. The asymmetry parameter R, except for the estimation of the distortion degree of the closest Eu^{3+}, is dependent on the JO parameter Ω_2 as well. Therefore, this relation was used for the estimation of the covalence level of the $Eu^{3+}-O^{2-}$ bond, delivering relevant information about short-range effects on the local environment of optically active ions.[39] It can be clearly seen that the covalence of the Eu−O bond decreases with an increase of the grain size.

Results of the luminescence kinetics studies performed at room temperature (see Table 3) gave nonexponential profiles of the decay times (see Figure 10). Thus, the effective emission decay times were calculated using the following equation:

$$\tau_m = \frac{\int_0^\infty tI(t)\,dt}{\int_0^\infty I(t)\,dt} \simeq \frac{\int_0^{t^{max}} tI(t)\,dt}{\int_0^{t^{max}} I(t)\,dt} \quad (10)$$

where $I(t)$ represents the luminescence intensity at time t corrected for the background and the integrals are evaluated in a range $0 < t < t^{max}$, where $t^{max} \gg \tau_m$. A general trend relying on the increase in the luminescence lifetime with the sintering temperature and/or grain growth was noticed. The lifetimes were equal to 1.42, 1.65, and 1.85 ms for samples heat-treated at 600, 700, and 800 °C, respectively. As a matter of fact, one should expect a longer decay for this type of compound characterized by the relatively long distance between neighboring Eu^{3+} ions. According to the reports of Zhu et al.,[14] the mean length of $Eu^{3+}-Eu^{3+}$ distances in $LiEu(PO_3)_4$ was 6.59 Å; thus concentration quenching caused by the ion−ion interaction is supposed to be significantly reduced. One of the possible explanations for such behavior in the system containing nanoparticles of $LiEu(PO_3)_4$ could be a high concentration of structural defects and superficial quenchers (O−H groups) in comparison to the single crystal of $LiEu(PO_3)_4$. This may be observed by studying nonexponential luminescence decay profiles that reflect the energy transfer from Eu^{3+} to the structural defects and/or OH groups. Probably in our samples, both factors are contributing to the increase in the

(37) Hreniak, D.; Strek, W.; Amami, J.; Guyot, Y.; Boulon, G.; Goutaudier, C.; Pazik, R. *J. Alloys. Compd.* **2004**, *380*, 348.
(38) Kiliaan, H. S.; Kotte, J. F. A. K.; Blasse, G. *Chem. Phys. Lett.* **1987**, *133*, 425.
(39) Capobianco, J. A.; Proulx, P. P.; Bettinelli, M.; Negrisolo, F. *Phys. Rev. B* **1990**, *42*, 5936.

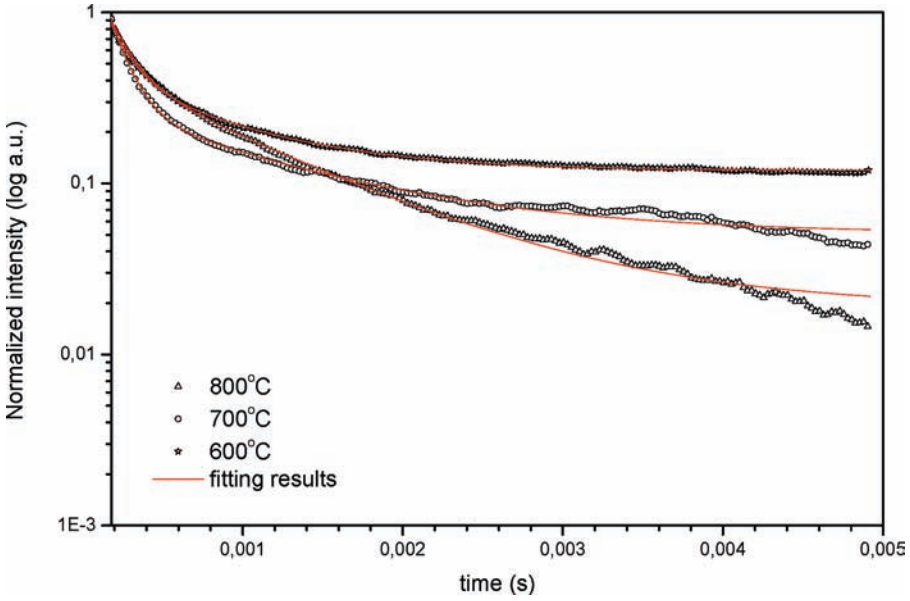

Figure 10. Decay time curves of $LiEu(PO_3)_4$ as a function of the sintering temperature measured at 300 K.

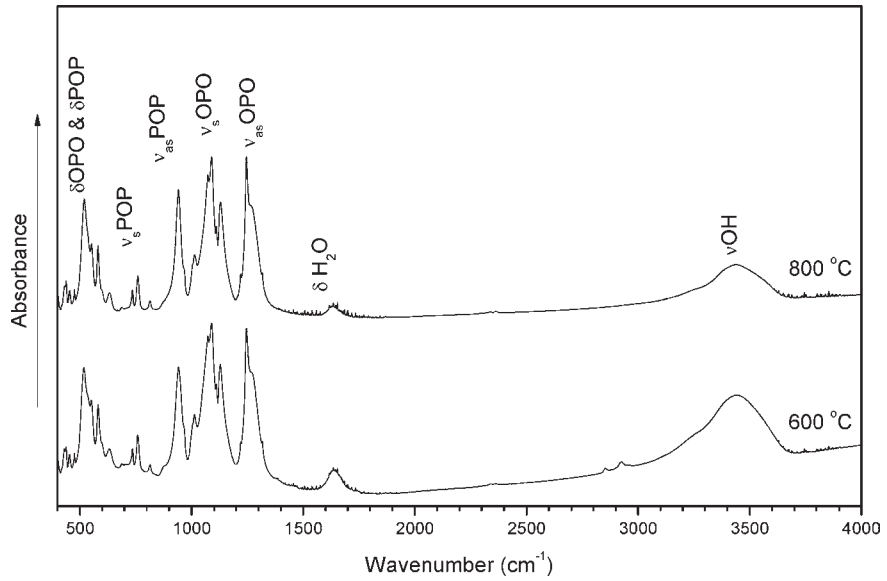

Figure 11. Representative IR spectra of the $LiEu(PO_3)_4$ nanoparticles.

nonradiative processes (see Table 3) with a simultaneous reduction of the grain size. In order to support that hypothesis, IR measurements were taken (see Figure 11), revealing the presence of strong and intense stretching vibrations of −OH groups at 3400 cm^{-1} and a scissoring mode of water molecules at 1630 cm^{-1} as well as other bands which correspond to the P−O−P or O−P−O vibrations. What is of great importance is that the intensity of water vibrations decreases with the increase in sintering temperature. Water removal under thermal treatment significantly increased the radiative decay rate A_{rad}, which directly enhanced the decay times of Eu^{3+}. In summary, the relatively short lifetimes of Eu^{3+} in $LiEu(PO_3)_4$ were caused by the quenching of the Eu^{3+} luminescence in $LiEu(PO_3)_4$ due to the high water content in the final product being at the same time a direct consequence of the chosen wet chemistry preparation route. Further thermal treatment should improve luminescence properties but at the cost of a significant increase in the grain size.

Conclusions

In the present work, we have reported, for the first time, the wet chemical synthesis and luminescence properties of $LiEu(PO_3)_4$ nanoparticles characterized by a mean grain size in the range of 30−50 nm dependent on the thermal treatment temperature. Since the biocompatibility of the inorganic phosphates is well-known, this material could be of possible interest in biorelated applications. The XRD and Raman spectroscopy confirmed the crystalline structure of the final product and allowed for its qualification to a similar chain type family of iso-structural polyphosphates. Significant contribution of the electron−phonon coupling was confirmed by the superposition of the Raman and emission spectra. A complex shape of the excitation spectra has been observed due to the thermal population of the $^7F_{1,2}$ levels as well as electron−phonon coupling. At least three components of the $^5D_0 \rightarrow {}^7F_0$ transition were found, indicating the

existence of more than one different crystallographic position of Eu^{3+}, instead of the one observed in the $LiEu(PO_3)_4$ single crystal. Structural defects, and therefore the possibility of finding the number of Eu^{3+} ions in unexpected positions and/or distorted sites, were responsible for the mentioned behavior. A slight blue shift of the $^5D_0 \rightarrow {}^7F_0$ band was noticed and ascribed to the size effect, corresponding to the change of crystal field energy. Splitting of the ^7F_J multiplet of Eu^{3+}, Rietveld analysis, and reasonable intensity of the $^5D_0 \rightarrow {}^7F_0$ transition suggested low symmetry (C_{2v}) of the closest environment of Eu^{3+}. The asymmetry parameter R was found to decrease with the grain growth, showing a relatively small degree of site distortion. Moreover, the covalence of the Eu−O bond decrease was correlated with the increase in the grain size. On the basis of the JO analysis, it was shown that the electric dipole mechanism decreases with an increase in the grain size and product crystallinity. The increase in decay times was related to the removal of water molecules and reduction of nonradiative energy transfer, being the responsible mechanism for luminescence quenching. Relatively short luminescence lifetimes are a consequence of the presence of structural defects and OH groups.

Acknowledgment. The authors would like to thank Mrs. L. Krajczyk for TEM and SAED images as well as Mr. M. Ptak for performing IR spectroscopy.